Alkali metal pyridinolate/piperidinolate pairs: A new type of materials for efficient reversible hydrogen storage

Alexis Munyentwali [a,b,1], Yang Yu [a,b,1], Xingchi Zhou [c], Wei Zhou [d], Qijun Pei [a,b], Khai C. Tan [a,b], Anan Wu [c,*], Hui Wu [d,*], Teng He [a,b,*], Ping Chen [a,b]

[a] Dalian Institute of Chemical Physics, Chinese Academy of Sciences, Dalian 116023, Liaoning, China
[b] Center of Materials Science and Optoelectronics Engineering, University of Chinese Academy of Sciences, Beijing 100049, China
[c] Fujian Provincial Key Laboratory of Theoretical and Computational Chemistry, College of Chemistry and Chemical Engineering, Xiamen University, Xiamen 361005, Fujian, China
[d] NIST Center for Neutron Research, National Institute of Standards and Technology, Gaithersburg, MD 20899-6102, United States

ARTICLE INFO

ABSTRACT

Chemical hydrogen storage in organic materials is a promising method thanks to its high storage density, reversibility, and safety. However, the dehydrogenation process of organic materials requires high temperatures due to their unfavorable thermodynamic properties. This study proposes a strategy to design a new type of hydrogen storage materials, i.e., alkali metal pyridinolate/piperidinolate pairs, by combining the effects of a heteroatom and an alkali metal in one molecule to achieve suitable dehydrogenation thermodynamics along with high hydrogen storage capacities. These air-stable compounds can be synthesized using low-cost reactants and water as a green solvent. Thermodynamic predictions indicate that enthalpy changes of dehydrogenation (ΔH_d) can be significantly reduced to the optimal range for efficient hydrogen release, exemplified by lithium 2-piperidinolate with a 5.6 wt% hydrogen capacity and a suitable ΔH_d of 32.2 kJ/mol-H_2. Experimental results obtained using sodium systems validate the computational predictions, demonstrating reversible hydrogen storage even below 100 °C. The superior hydrogen desorption performance of alkali metal piperidinolates could be attributed to their suitable ΔH_d induced by the combined effect of ring nitrogen and metal substitution on their structures. This study not only reports new low-cost hydrogen storage materials but also provides a rational design strategy for developing metalorganic compounds possessing high hydrogen capacities and suitable thermodynamics for efficient hydrogen storage.

1. Introduction

Hydrogen is considered to be a promising energy carrier due to its high gravimetric energy density and carbon-free nature [1–3]. However, the lack of efficient hydrogen storage and transportation methods, mainly due to its low volumetric energy density, constitutes the Achilles' heel for hydrogen widespread application [4,5]. Compared to the traditional storage methods, such as high-pressure compression and liquefaction, chemical hydrogen storage in condensed materials has been identified to be an effective solution to this challenge, as it allows safe and efficient high-capacity hydrogen uptake and release through controllable thermal or catalytic processes [6,7].

Several types of materials for chemical hydrogen storage have been developed, including metal hydrides [8,9], chemical hydrides [10], complex hydrides [11], and liquid organic hydrogen carriers (LOHCs) [12,13]. However, up to date, no materials have yet been developed to meet all the requirements for practical application. The reason may be that "high hydrogen capacity" and "suitable thermodynamics of dehydrogenation", two essential properties for reversible hydrogen storage, are very challenging to achieve concurrently in one material. Therefore, a breakthrough in developing novel material systems is highly needed.

Among existing hydrogen storage materials, LOHCs have been proposed as a promising solution for large-scale and long-

---

distance hydrogen transportation. In the quest to develop ideal LOHC systems, it has been demonstrated that the incorporation of heteroatoms, such as nitrogen (N) in cycloalkanes rings, could improve the thermodynamics of dehydrogenation (ring N effect) [14,15]. However, drawbacks such as unfavorable thermodynamics, sluggish kinetics, low dehydrogenation selectivity, and high cost still limit the application of reported LOHCs.

By leveraging the rich chemistry of organic materials, recently, our research group introduced new hydrogen storage materials identified to constitute a new type of metalorganic compounds (MOCs). These compounds are formed via the substitution of protic H on organic molecules by lightweight alkali or alkaline earth metals such as Li, Na, and K [16]. Interestingly, thanks to the strong electron-donating ability of these metals to modulate the electron densities of organic compounds, this "metal substitution approach" has shown great potential in improving dehydrogenation thermodynamics. For instance, lithium carbazolide has an enthalpy change of dehydrogenation (ΔH_d) of 34.2 kJ/mol-H_2, which is an ideal thermodynamic parameter for efficient hydrogen storage [17]. However, the reported MOCs still have notable drawbacks, such as high synthesis costs due to the use of metal hydrides and costly organic substrates, low stability in air, and slow kinetics caused by mass transfer limitations [17–19]. Therefore, further research is highly needed to develop novel and more efficient MOCs for practical hydrogen storage.

Inspired by the strategies of "heteroatom incorporation" and "metal substitution" in LOCHs and MOCs, respectively, this study combined the effects of the two strategies in one molecule to develop new high-capacity hydrogen storage materials with improved dehydrogenation thermodynamics. To achieve this objective, three positional isomers of the pyridinol structure were utilized as parent substrates that can give, upon metal substitution, MOCs possessing both N-atom in the ring and alkali metals as substituents on the ring (Fig. 1a). Furthermore, to address the cost and stability issues faced by our previously reported MOCs, metal hydrides and inert atmosphere were not needed in the present study, indicating a significant cost reduction.

Thermodynamic predictions revealed that ΔH_d values of all alkali metal piperidinolates are lower than those of their parent piperidinols, and most of them fall within the optimum range for efficient hydrogen storage [20,21]. In addition, the experimental H_2 desorption performance trend was consistent with theoretical ΔH_d. The superior H_2 desorption performance of alkali metal piperidinolates, compared to their parent piperidinols and analogous cyclohexanolates, could be attributed to their suitable ΔH_d induced by the combined effect of ring N and metal substitution on their structures. Therefore, this study not only reports novel low-cost hydrogen storage materials but also provides a rational design strategy for developing MOCs possessing high hydrogen storage capacities and optimal thermodynamics for efficient reversible hydrogen storage.

2. Results and discussion

2.1. Material design and thermodynamic predictions

Alkali metal pyridinolate/piperidinolate pairs were designed as novel hydrogen storage materials possessing both a N atom within the ring and an alkali metal as part of an electron-donating substituent outside the ring (Fig. 1a). This new structure optimization strategy was hypothesized to lead to better dehydrogenation thermodynamics on account of the synergy of the ring N and metal substitution effects. To this end, we considered three positional isomers of the pyridinol structure: 2-pyridinol (2-OH-pyr), 3-pyridinol (3-OH-pyr), and 4-pyridinol (4-OH-pyr) as H-lean

substrates; and three positional isomers of the piperidinol structure: 2-piperidinol (2-OH-pip), 3-piperidinol (3-OH-pip), and 4-piperidinol (4-OH-pip) as H-rich substrates. The substitution of protic H in these compounds by Li, Na, or K could lead to 3 pairs of MOCs for every metal atom (Fig. S1). For instance, in the case of sodium, these pairs are sodium 2-pyridinolate/sodium 2-piperidinolate (2-NaO-pyr/2-NaO-pip), sodium 3-pyridinolate/sodium 3-piperidinolate (3-NaO-pyr/3-NaO-pip), and sodium 4-pyridinolate/sodium 4-piperidinolate (4-NaO-pyr/4-NaO-pip).

To investigate the effect of combining ring N and metal substitution on dehydrogenation thermodynamics, the enthalpy change of dehydrogenation (ΔH_d) was considered as a thermodynamic metric. Then, we employed X1s, a density-functional theory (DFT)-based method that combines B3LYP with neural network correction [22], to predict gas-phase ΔH_d of all Li, Na, and K piperidinolates. Moreover, these ΔH_d values of alkali metal piperidinolates were compared to those of pristine piperidinols and analogous cyclohexanolates as two related reference structures. Thermodynamic calculations revealed that ΔH_d values of all alkali metal piperidinolates are lower than those of their parent piperidinols (Fig. 1b). This phenomenon could be attributed to the strong electron-donating ability of alkali metals to reduce ΔH_d. However, consistent with our previous studies [16,17], the extent of ΔH_d reduction was found to depend on the Pauling electronegativity (Z) of the alkali metal. Specifically, the lower the electronegativity of the alkali metal, the more significant the reduction in the dehydrogenation enthalpy (Fig. 1b). Hence, K-piperidinolates have the lowest ΔH_d compared to the Na and Li counterparts. For instance, while the ΔH_d of 4-KO-pip is only 62.1% of the pristine 4-OH-pip ΔH_d, those of 4-NaO-pip and 4-LiO-pip are 64.2% and 83.7%, respectively (Fig. 1b). To better understand the effect of alkali metal substitution on reducing ΔH_d, calculations of natural bond orbital (NBO) charges were performed on pyridinols and sodium pyridinolates. The results showed that the charges in the aromatic rings of the pyridinolates are negative or less positive compared to those in the rings of their parent pyridinols (Table S1). Given that Na donates more electrons than H to O, this finding suggests that electrons donated by sodium during the substitution of protic H delocalize across the ring structures through a strong p-π conjugation, which then stabilizes sodium pyridinolates by the enhanced aromaticity. It should be noted that although alkali metals could also stabilize piperidinolates through a hyperconjugation effect, its magnitude is smaller than that of p-π conjugation in pyridinolates. Therefore, the superior stability of pyridinolates over piperidinolates automatically renders the dehydrogenation reaction more thermodynamically favorable, justifying why the ΔH_d values of piperidinolates are lower than those of their parent piperidinols.

Another crucial observation is the common pattern of ΔH_d variation among positional isomers for all Li, Na, and K compounds. The *ortho* isomers (1,2 arrangement) exhibit the lowest ΔH_d, followed by *para* isomers (1,4 arrangement), while *meta* isomers (1,3 arrangement) display the highest ΔH_d. This is exemplified by the comparison between K compounds. 3-KO-pip and 4-KO-pip have ΔH_d of 44.13 and 35.15 kJ/mol-H_2, respectively. On the other hand, ΔH_d of 2-KO-pip is only 27.71 kJ/mol-H_2, which is so far the lowest, and probably, the most suitable ΔH_d achieved by a metalorganic compound. This finding could be explained by the fact that different arrangements of atoms in structural isomers can lead to different electron density distributions (Table S1), thereby causing the isomers to react differently as also reported in the literature [23,24]. Hence, it can be concluded that in the case of alkali metal pyridinolate/piperidinolate systems, significant ΔH_d reduction only occurs in *ortho* and *para*-positional isomers.

Furthermore, the reported "ring N effect" [15] was tested and confirmed not only on piperidinols but also on alkali metal
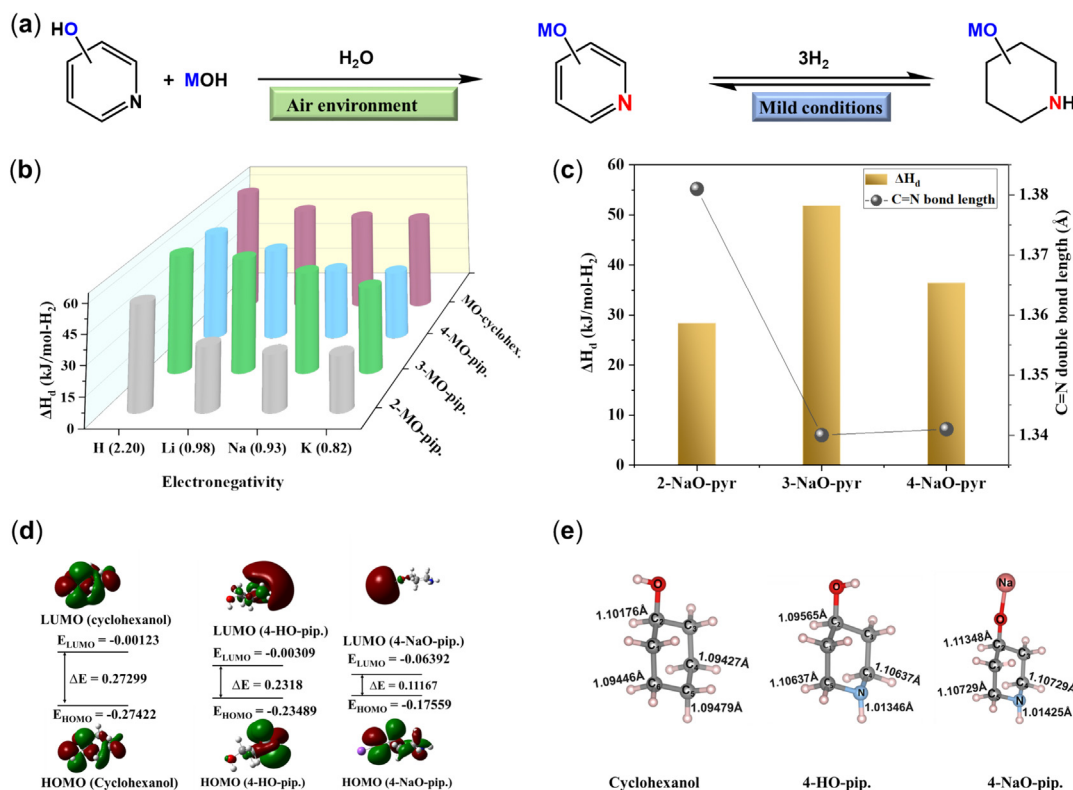
Fig. 1. (a) Concept of the study: facile and low-cost synthesis of alkali metal pyridinolates and reversible hydrogen storage under mild conditions. M: Li, Na, or K. (b) Calculated enthalpy changes of dehydrogenation (ΔH_d) in kJ/mol-H_2 for alkali metal piperidinolates vs. electronegativity (Z) of the alkali metals. For comparison, ΔH_d of parent piperidinols and analogous metal cylohexanolates (MO-cylohex.) is also presented. (c) ΔH_d of Na-piperidinolates vs. C=N double bond length in Na-pyridinolates. (d) Comparison of HOMO-LUMO band gap between cyclohexanol, 4-HO-pip, and 4-NaO-pip. (e) Comparison of C–H bond length between cyclohexanol, 4-OH-pip, and 4-NaO-pip.

piperidinolates. As illustrated in Fig. 1(b), all piperidinol isomers have lower ΔH_d than cyclohexanol. Besides, it is noticeable that ΔH_d values of all *ortho* and *para* isomers of Li, Na, and K piperidinolates are lower than those of their analogous cyclohexanolates. Therefore, by comparing the molecular structures of alkali metal piperidinolates to those of their parent piperidinols and analogous cylohexanolates, it is plausible to attribute the low ΔH_d of alkali metal piperidinolates, especially *ortho* and *para* isomers, to the effective synergy of ring N and metal substitution effects on their structures. It is also important to mention that apart from the strong electron-donating ability of alkali metals to modulate the dehydrogenation thermodynamics, their presence in MOCs has another crucial implication of leading to high hydrogen storage capacities owing to their lightweight. For instance, 2-LiO-pyr/2-LiO-pip pair has a ΔH_d of 32.2 kJ/mol-H_2 in addition to its high H_2 storage capacity of 5.6 wt%.

To gain more insights into these observed suitable dehydrogenation thermodynamics of alkali metal pyridinolate/piperidinolate pairs, we investigated the relationship between ΔH_d and some molecular properties known to affect reaction thermodynamics and kinetics [25,26]. For instance, Fig. 1(c) shows that a longer C=N double bond in sodium pyridinolates corresponds to a lower ΔH_d, indicating a more favorable thermodynamic equilibrium to achieve reversible hydrogen storage under mild conditions for alkali metal pyridinolate/piperidinolate pairs with low ΔH_d, such as 2-NaO-pyr/2-NaO-pip and 2-LiO-pyr/2-LiO-pip systems. Additionally, computational data demonstrate that the highest occupied molecular orbital- lowest unoccupied molecular orbital (HOMO-LUMO) band gap decreases progressively from cyclohexanol to 4-OH-pip and becomes significantly narrower in 4-NaO-pip (Fig. 1d). Although the HOMO-LUMO band gap is

conventionally regarded as an indicator of kinetic stability, with a larger gap correlating with higher stability [26], the trend of this band gap between cyclohexanol, 4-OH-pip, and 4-NaO-pip (which is identical for all MO-pip isomers) is consistent with ΔH_d data (Fig. 1b), suggesting enhanced reactivity of the MOCs.

Similarly, the comparison of C–H bond length between cyclohexanol, 4-OH-pip, and 4-NaO-pip revealed that both the incorporation of the N atom in the ring and the substitution of protic H by sodium lead to the elongation of C–H bond, especially in α and γ positions where the first C–H bond dissociation is very likely to eventuate during the dehydrogenation process (Fig. 1e). All these findings collectively indicate the effectiveness of the synergy of ring N and alkali metal substitution effects on fine-tuning both the thermodynamics and kinetics of the MOCs for efficient hydrogen storage.

2.2. Material synthesis, characterizations, and crystal structures

By considering the optimal trade-off between ΔH_d and H_2 storage capacity, which is a significant material aspect for practical H_2 storage application [6], Na-substituted compounds were selected as representative materials to be synthesized and subsequently utilized to validate the computational findings experimentally. All these materials, except 2-NaO-pip, were initially synthesized by reacting their organic substrates with sodium hydride (NaH) in a 1:1 M ratio at 60 °C in tetrahydrofuran (THF) solvent under an inert atmosphere (Fig. S1). In each synthesis, *ca.* one equivalent H_2 gas was released, indicating a complete conversion. 2-NaO-pip could not be synthesized because its precursor (2-piperidinol) was not commercially available. It is worth noting that H-lean sodium compounds could also be synthesized at room temperature

in the air environment. This facile and cost-effective alternative method, which involves using NaOH as a more convenient base and water as an environmentally friendly solvent (Fig. 1a), is feasible thanks to the acidic character of pyridinols (Table S2).

Sodium-substituted compounds were characterized using liquid-state nuclear magnetic resonance (NMR) spectroscopy. ^{1}H NMR spectra of H-lean compounds (Fig. 2a) and the H-rich counterparts (Fig. 2b) show the disappearance of the OH group proton, which is an indicator of a successful metal substitution. In addition, proton resonances in sodium-substituted compounds, especially H-lean, clearly shifted upfield compared to their counterparts in the organic substrates. This observation indicates a more shielding effect attributed to the strong electron-donating ability of sodium, which increased electron density in the aromatic ring as revealed by the calculations of natural bond orbital (NBO) charges (Table S1). It is important to mention that in the case of H-rich compounds, this upfield shift is not as apparent as the one observed in H-lean compounds. This difference arises from the fact that electrons transferred from the metal to the aromatic ring of H-lean compounds are more easily delocalized through a strong p-π conjugation compared to those in H-rich compounds whose delocalization stems from a weak hyperconjugation effect.

Furthermore, sodium pyridinolates and piperidinolates display a similar single sharp peak in their ^{23}Na NMR spectra (Fig. 2c), which is additional evidence of a successful metal substitution. The Na peak in sodium-substituted compounds shifted slightly from the peak in the NaOH sample, indicating that it is not due to any residual NaH/NaOH but rather to the Na atom that replaced the labile proton during the synthesis. ^{13}C NMR characterization of both H-lean and H-rich sodium-substituted compounds shown in Figs. S2 and S3, respectively, also indicates the effect of metal substitution. Generally, carbon atoms close to the N atom and ONa group in sodium-substituted compounds have a downfield shift compared to their counterparts in the pristine pyridinols and piperidinols. However, the fact that carbon atoms in sodium-substituted compounds shifted differently in the isomers indicates different electronic properties as revealed by NBO charges (Table S1). These findings can reasonably justify the observed difference in their enthalpy changes of dehydrogenation (Fig. 1b).

The synthesized MOCs were also characterized by powder X-ray diffraction (PXRD), as shown in Fig. S4 (H-lean) and Fig. S5 (H-rich). XRD patterns of all sodium-substituted compounds are very distinct from those of their organic precursors, indicating the formation of new phases. In addition, sodium-substituted compounds were tested for air and moisture stability, one of the most indispensable qualities of potential hydrogen storage materials. Encouragingly, sodium pyridinolates possess outstanding air and moisture stability. Fig. 2(d) shows the similarity between XRD patterns of a 4-NaO-pyr fresh sample prepared under an inert atmosphere and one exposed to air for a month. To demonstrate that H-lean MOCs can be effectively produced via a facile and low-cost alternative method using metal hydroxides instead of metal hydrides, Fig. 2(d) also illustrates the similarity between XRD patterns of a 4-NaO-pyr sample synthesized with NaH in THF and one made with NaOH in H$_2$O. This similarity was also confirmed by ^{1}H NMR (Fig. S6). It is noteworthy that the high stability of hydrogen storage materials in air and low-cost synthesis are important factors for practical application, highlighting the great potential of alkali metal pyridinolates for large-scale hydrogen storage.

Attempts were made to determine the structures of sodium pyridinolates, but we only managed to solve the crystal structure of 4-NaO-pyr (Fig. 3). The laboratory XRD pattern of 4-NaO-pyr can be indexed to a monoclinic structure with space group $P2_1/a$ (No.14). The crystal structure was solved using direct space methods with the first-principles molecular dynamics simulated annealing performed to confirm the 4-C$_5$H$_4$NO$^-$ configuration with the lowest energy. Due to the inadequate number of observations in the laboratory XRD data, the 4-C$_5$H$_4$NO$^-$ was kept as a rigid body during Rietveld refinement and the bond lengths discussed below are from the relaxed structure. The C$_5$H$_4$NO$^-$ rigid body together with the cation positions and lattice parameters were refined. The Rietveld fit to the XRD pattern is shown in Fig. 3(a). Refined lattice parameters of NaOC$_5$H$_4$N are a = 12.0684(10) Å, b = 11.4875(9) Å, c = 3.64095(19) Å, β = 92.427(6)°, and V = 504.31(8) Å^3. Additional crystallographic details can be found in the CIF file deposited to the Cambridge Structural Data Center (CCDC) under deposition number CCDC 2372009.

In the 4-NaO-pyr structure (Fig. 3b and c), each Na is bonded with three surrounding 4-C$_5$H$_4$NO$^-$ through Na–O bonds and two 4-C$_5$H$_4$NO$^-$ through Na–N bonds, leading to a square pyramid coordination geometry with bond lengths of 2.304–2.440 Å and 2.588–2.601 Å for Na–O and Na–N, respectively. As shown in Fig. 3(b), the Na cations are connected by O atoms and align themselves, forming Na–O double zigzag chains along c direction.

The 4-C$_5$H$_4$NO$^-$ units are linked together through O and N by these Na–O double zigzag chains, constructing rectangular channels propagating along c direction with the aromatic rings as the channel walls and Na–O double zigzag chains as the pivot pillars. The neighboring rectangle channels are interlocked together as jigsaw puzzles and spread along a and b directions, forming a three-dimensional (3D) network. Furthermore, as shown in Fig. 3(b and c), the C$_5$H$_4$-NO$^-$ groups could bond with the strong electron-donating Na cation through both Na–O and Na–N, which would help electron delocalization and enhance the aromaticity of C$_5$H$_4$NO$^-$ more compared to that of C$_6$H$_5$O$^-$ in sodium phenoxide (NaOC$_6$H$_5$), where C$_6$H$_5$O$^-$ groups interact with Na only through O (Fig. 3d). On the other hand, both ring N and metal substitution have effects on weakening adjacent C–H bonds in the H-rich molecules as reported in the literature [15,16] and also confirmed by the present study (Fig. 1e). Therefore, the presence of ONa group and N atom in *para* position (1,4) within 4-NaO-pip could weaken most of the C–H bonds, whereas C–H bond weakening could only occur at positions adjacent to ONa in Na-cyclohexanolate (NaOC$_6$H$_{11}$) (Fig. 1e). Consequently, the superior stability of 4-NaO-pyr and weaker C–H bonds in 4NaO-pip would result in an overall reduced endothermic dehydrogenation enthalpy (ΔH_d) of the 4-NaO-pip/4-NaO-pyr pair compared to that of the Na-phenoxide/Na cyclohexanolate (Fig. 1b).

2.3. Reversible hydrogen storage in solid state

After synthesizing sodium pyridinolate/piperidinolate pairs, these materials were experimentally studied to evaluate their hydrogen desorption performance and test the proposed synergetic effect of ring N and alkali metal substitution. Due to the lack of 2-OH-pip precursor, 2-NaO-pip/-2NaO-pyr pair was excluded from subsequent experiments despite having the lowest ΔH_d among other sodium pyridinolates/sodium piperidinolate pairs.

Hydrogen desorption experiments were initially conducted in a solid state to exclude solvent effects. Since 4-NaO-pip/4-NaO-pyr possesses an excellent theoretical ΔH_d (36.4 kJ/mol-H$_2$), 4-NaO-pip was utilized for catalysts screening and optimization of H$_2$ desorption conditions. Fig. 4(a) illustrates the H$_2$ desorption profiles of 4-NaO-pip catalyzed by different supported metal catalysts from room temperature to 140 °C. Among these catalysts, 5% Rh/C exhibited the highest activity to the extent of enabling 4-NaO-pip to release 4.4 wt% H$_2$ per 4-NaO-pip molecule after 22 h, compared to its theoretical H$_2$ storage capacity of 4.9 wt%. Encouragingly, 2.0 wt% and 4.1 wt% H$_2$ were released only after 1 and 4 h, respectively, indicating fast initial rates. To confirm the dehydrogenation of 4-NaO-pip, ^{1}H NMR characterization of a sample recovered from the H$_2$ desorption test showed a near-full conversion of the substrate and a complete selectivity to 4-NaO-pyr
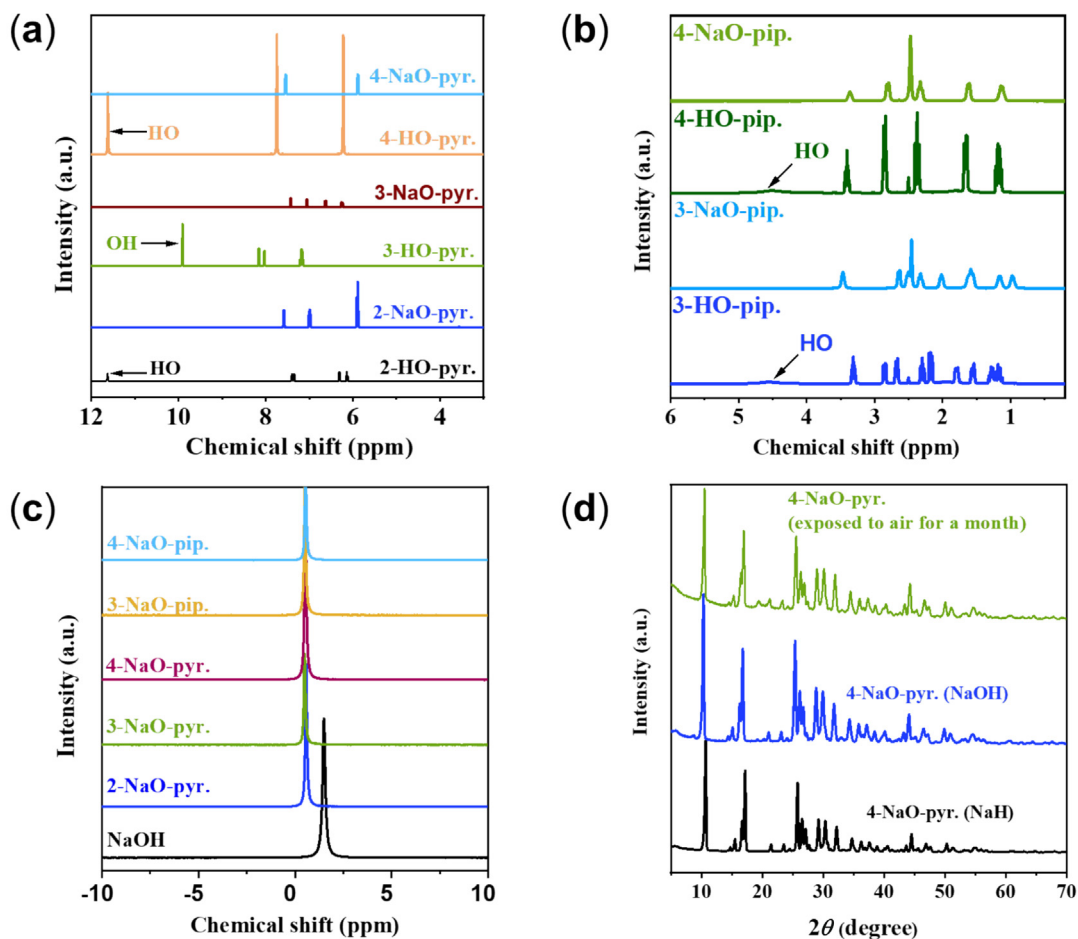
Fig. 2. (a) ^{1}H NMR spectra of sodium pyridinolates and their parent pyridinols in DMSO d6 . (b) ^{1}H NMR spectra of sodium piperidinolates and their parent piperidinols in DMSO d6 . (c) ^{23}Na NMR spectra of sodium pyridinolates and piperidinolates compared to NaOH in D$_2$O. (d) Comparison between XRD patterns of 4-NaO-pyr samples synthesized using NaH in THF and NaOH in H$_2$O. These 4-NaO-pyr fresh samples are also compared to a 4-NaO-pyr (NaOH) sample exposed to air for a month.

(Fig. S7). These findings prompted us to investigate the temperature profile of 4-NaO-pip releasing H$_2$ in detail.

Impressively, temperature-programmed desorption coupled with mass spectroscopy (TPD-MS) revealed that 4-NaO-pip starts releasing H$_2$ at temperatures as low as 60 °C. In a TPD-MS experiment conducted from room temperature to 200 °C, H$_2$ release peaked and levelled off at 102 and 160 °C, respectively (inset of Fig. 4b), and no other gases were detected (Fig. S8). In an attempt to examine if 4-NaO-pip could release a considerable amount of H$_2$ at low temperatures, H$_2$ desorption was subsequently studied from room temperature to 100 °C using the 5% Rh/C catalyst. As shown in Fig. 4(b), hydrogen capacity as high as 4.0 wt% could be reached at 100 °C in 65 h. Interestingly, 2.6 wt% H$_2$ could be released within the initial 4h, once again indicating fast initial rates.

It should be noted that the observed long total reaction times during these H$_2$ desorption experiments may be attributed to the deactivation/poisoning of noble metal-based catalysts in the reactions of N-heterocycles [28,29] and/or sluggish kinetics in solid-state reactions [1]. To verify if the trend of the calculated ΔH_d data could be experimentally reflected in H$_2$ desorption performance, 4-NaO-pip was compared to the related H-rich compounds, namely 3-NaO-pip, 4-OH-pip, and Na-cyclohexanolate. However, 4-OH-pip could not be tested in solid-state dehydrogenation because both its melting and boiling points are below the reaction temperature (140 °C). As shown in Fig. 4(c) and Fig. S9, 4-NaO-pip displayed superior H$_2$ desorption performance by outperforming Na-cyclohexanolate and 3-NaO-pip in terms of desorbed H$_2$ under

identical experimental conditions. It is important to note that the H$_2$ desorption performance of these materials, which have the same theoretical H$_2$ storage capacity (4.9 wt%), followed a trend similar to the one of calculated ΔH_d (Fig. 4c). Although these H$_2$ desorption kinetic experiments were conducted under vacuum, which arguably affected thermodynamic equilibria, the similarity of H$_2$ desorption performance and theoretical ΔH_d trends could reasonably enable us to attribute the superior performance of 4-NaO-pip to its favorable dehydrogenation thermodynamics.

Furthermore, after 4-NaO-pip demonstrated significant H$_2$ desorption performance in the solid state, its H-lean form (4-NaO-pyr) was subsequently evaluated for H$_2$ absorption to assess the potential of the 4-NaO-pyr/4-NaO-pip pair in terms of reversible H$_2$ storage. Fig. 4(d) shows the H$_2$ absorption profiles of 4-NaO-pyr at 140 °C, catalyzed by Rh/C and Rh/Al$_2$O$_3$, two catalysts that exhibited the best performance during H$_2$ desorption tests on 4-NaO-pip. By and large, 4-NaO-pyr H$_2$ absorption in the solid state faced a challenge of slow kinetics that particularly required high catalyst loading and high H$_2$ pressure to reach significant conversion rates. Under these conditions, 5% Rh/Al$_2$O$_3$ displayed a better hydrogenation activity, enabling 4-NaO-pyr to achieve complete hydrogenation as confirmed by ^{1}H NMR (Fig. S10).

2.4. Reversible hydrogen storage in aqueous solution

Given the sluggish kinetics of hydrogen uptake and release observed in the solid-state experiments, reversible
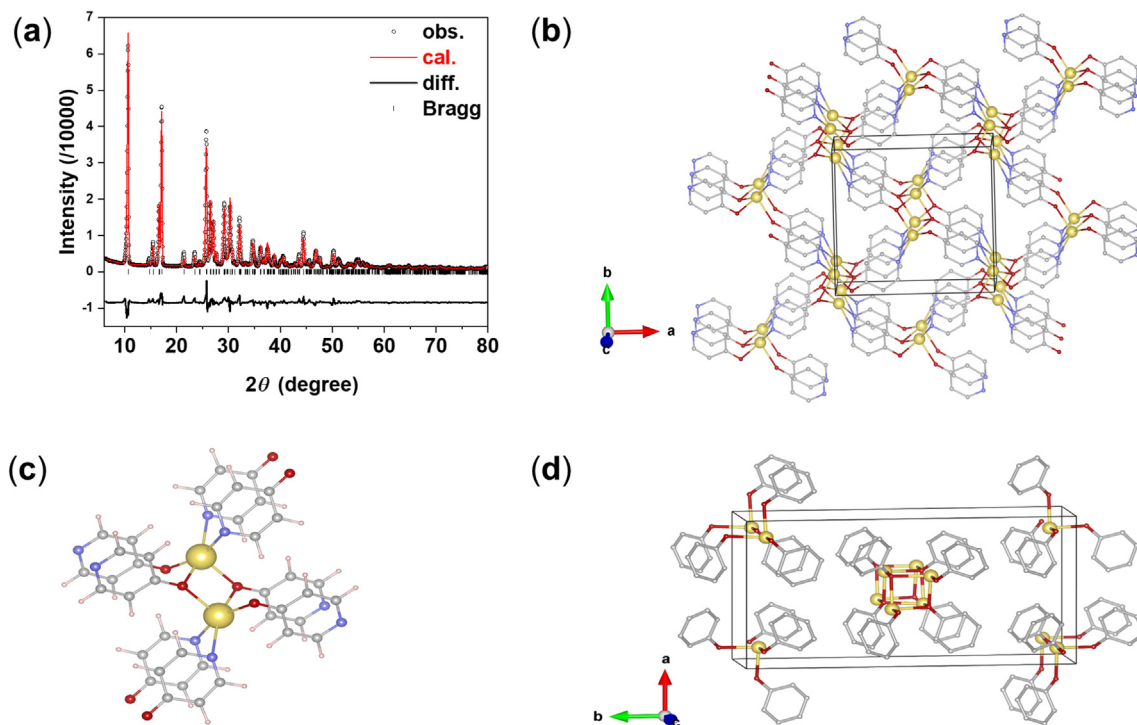
Fig. 3. (a) The Rietveld fit to the XRD pattern of 4-NaO-pyr. Experimental (circles), fitted (line), and difference (line below observed and calculated patterns). Vertical bars indicate the calculated positions of Bragg peaks. Rwp = 0.0964, Rp = 0.0725, and χ^2 = 5.38. (b) 4-NaO-pyr crystal structure. H atoms are omitted for clarity. (c) Local coordination of Na^+ in 4-NaO-pyr structure. Yellow balls: Na, red balls: O, grey balls: C, blue balls: N, tan balls: H atoms. (d) Na-phenoxide crystal structure used with permission from reference [27].
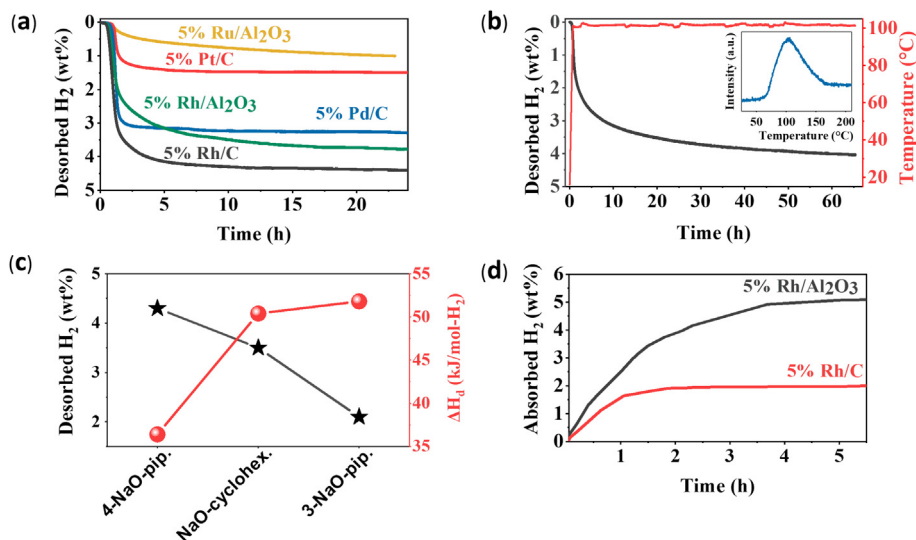

Fig. 4. (a) 4-NaO-pip H_2 desorption catalyzed by different catalysts, temperature: 25–140 °C. (b) 4-NaO-pip H_2 desorption catalyzed by 5% Rh/C, temperature: 25–100 °C. Inset: TPD-MS of 4-NaO-pip with 5% Rh/C. (c) A comparison of H_2 desorption performance achieved after 10 h of reaction time vs. calculated ΔH_d between 4-NaO-pip, 3-NaO-pip, and Na-cyclohexanolate (abbreviated as NaO-cyclohex.), temperature: 25–140 °C, catalyst: 5% Rh/C. (d) 4-NaO-pyr H_2 absorption catalyzed by 5% Rh/Al$_2$O$_3$ in a solid state, pressure: 60 bar H_2, substrate: metal molar ratio (2:1), temperature: 140 °C.

hydrogen storage was subsequently examined in the liquid solution phase using water as a green solvent. Interestingly, the dehydrogenation of 4-NaO-pip catalyzed by 5% Rh/C could reach a conversion of 92.6% just after 12 h at 100 °C (Fig. 5a). Extending the reaction time up to 18 h led to an excellent conversion of 99.8% with 100% selectivity to 4-NaO-pyr (Fig. S11). According to ex-situ NMR characterization of samples taken throughout the reaction time, including samples taken at initial reaction times as

early as 20 min, no other signals apart from those of the initial substrate (4-NaO-pyr) and fully hydrogenated product (NaO-pip) were observed; indicating no detectable reaction intermediate(s) or side product(s) (Figs. S11 and S12). The catalytic dehydrogenation reactions of 3-NaO-pip, 4-OH-pip, and Na-cyclohexanolate were also examined and compared to 4-NaO-pip under identical experimental conditions (Fig. 5b). Impressively, 4-NaO-pip also achieved the highest conversion as it was the case in the solid-state
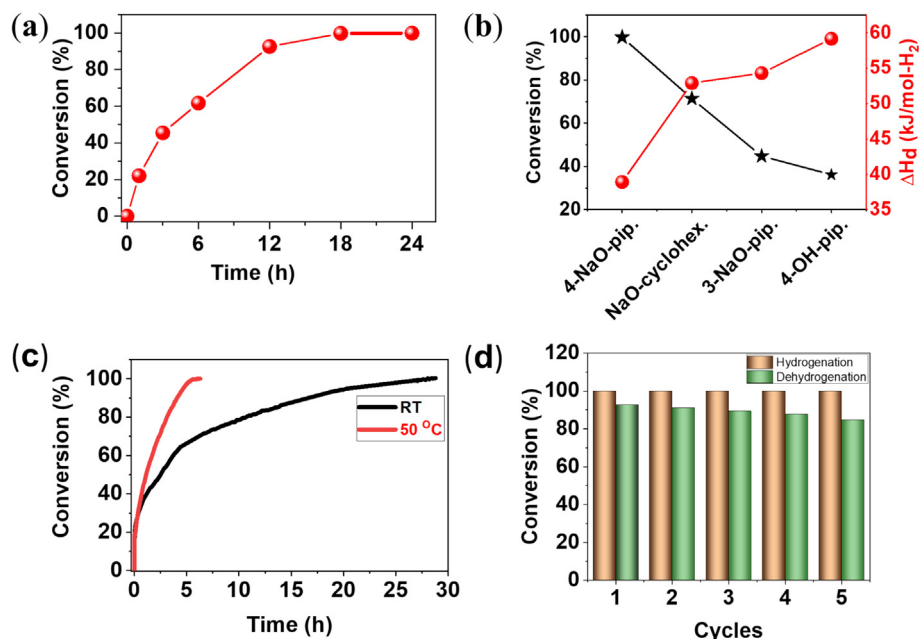
Fig. 5. (a) Dehydrogenation of 4-NaO-pip catalyzed by 5% Rh/C in aqueous solution at 100 °C. Conversion was determined using ^{1}H NMR. (b) A comparison of conversion after 18 h of reaction time vs. calculated ΔH_d between 4-NaO-pip and other reference H-rich compounds of this study. (c) Hydrogenation of 4-NaO-pyr catalyzed by 5% Rh/C in aqueous solution at room temperature and 50 °C, 40 bar H_2 pressure. (d) Hydrogenation and dehydrogenation cycles for the 4-NaO-pyr/4-NaO-pip pair in aqueous solution at 100 °C using 5% Rh/C as a bidirectional catalyst. Hydrogenation time: 4 h, dehydrogenation time: 14 h.

dehydrogenation experiments (Fig. 4c). The most fascinating result from the data depicted in Fig. 5(b) is probably the similarity of the ΔH_d and conversion trends among the studied materials.

In addition, the catalytic dehydrogenation results presented in Fig. 5(b) enabled us to test the hypothesis of the present study conclusively. In line with the thermodynamic predictions (Fig. 1b), 4-NaO-pip demonstrated superior H_2 desorption performance compared to Na-cyclohexanolate under identical conditions, as evidenced in both solid-state (Fig. 4c) and aqueous solution experiments (Figs. S11 and S13). Considering the structures of these two molecules, the superior H_2 desorption performance of 4-NaO-pip could be attributed to the presence of the N atom in its structure (ring N effect). Similarly, 4-NaO-pip outperformed 4-OH-pip during experimental catalytic dehydrogenation in aqueous solution (Figs. S11 and S13). Since the structure of 4-NaO-pip differs from that of 4-OH-pip only in the Na atom, a possible explanation for the superior H_2 desorption performance of 4-NaO-pip might be the effect of metal substitution. Taken together, the comparison of 4-NaO-pip to 4-OH-pip and Na-cyclohexanolate shows that its superior H_2 desorption performance could be attributed to its low ΔH_d induced by the combined effect of metal substitution and the incorporation of the N atom on its structure.

Furthermore, to test the hydrogen storage reversibility of the 4-NaO-pyr/4-NaO-pip pair in aqueous solution, hydrogenation of 4-NaO-pyr was evaluated using 5% Rh/C. Impressively, the catalyst could achieve full hydrogenation of 4-NaO-pyr even at room temperature and under a moderate H_2 pressure of 40 bar after 28 h (Fig. S14). This complete hydrogenation was achieved along with 100% selectivity to 4-NaO-pip as revealed by ^{1}H NMR (Fig. S15) and ^{13}C NMR (Fig. S16). Increasing the reaction temperature up to 50 °C could lead to a full hydrogenation of 4-NaO-pyr only after 6 h (Fig. S14).

Lastly, after confirming the reversibility of the 4-NaO-pyr/4-NaO-pip pair in H_2 storage through separate hydrogenation and dehydrogenation processes, its ability to realize multiple hydrogenation/dehydrogenation cycles was also tested in an aqueous media using 5% Rh/C as a bidirectional catalyst. Although the catalyst could not achieve full conversion during 14 h of dehydrogenation steps, unlike in their fast hydrogenation counterparts, the pair still accomplished five cycles with good H_2 uptake and release cycling stability (Fig. 5d). Besides, ex-situ ^{1}H NMR characterization of samples taken after each cycle step did not show any material decomposition (Fig. S17), indicating excellent stability of the 4-NaO-pyr/4-NaO-pip pair over multiple hydrogenation and dehydrogenation cycles. However, considering the observed sluggish dehydrogenation kinetics, further efforts are crucial to developing more efficient catalysts for realizing the full potential of this promising reversible hydrogen storage system.

3. Conclusions

This study was conducted to design, synthesize, and experimentally investigate alkali metal pyridinolate/piperidinolates pairs as new and low-cost materials for efficient reversible hydrogen storage. DFT calculations demonstrated that the enthalpy changes of dehydrogenation (ΔH_d) of alkali metal piperidinolates are lower than those of their parent piperidinols. In particular, lithium 2-piperidinolate (2-LiO-pip) with a high H_2 capacity of 5.6 wt% possesses an ideal ΔH_d of 32.2 kJ/mol-H_2. Results from H_2 desorption experiments conducted in solid state and aqueous media using sodium pyridinolate/piperidinolate pairs were in full agreement with computational predictions. For instance, sodium 4-piperidinolate (4-NaO-pip) experimentally outperformed its parent piperidinol (4-OH-pip) and Na-cyclohexanolate in H_2 desorption. This superior H_2 desorption performance of 4-NaO-pip could be attributed to its low ΔH_d induced by the combined effect of ring N and alaki metal substitution on its structure. Additionally, sodium 4-pyridinolate (4-NaO-pyr), which can be synthesized from low-cost chemicals via a facile method, could be fully hydrogenated under mild conditions, highlighting the great potential of the 4-NaO-pyr/4-NaO-pip system for reversible H_2 storage. However, efficient catalysts are still needed to improve the kinetics and cyclability for practical application. Overall, this study not only

reports new low-cost hydrogen storage materials but also provides a rational design strategy for developing metalorganic compounds possessing suitable thermodynamics for efficient reversible hydrogen storage.

Experimental section

Experimental details can be found in the Supporting Information.

CRediT authorship contribution statement

Alexis Munyentwali: Data curation, Formal analysis, Investigation, Methodology, Writing – review & editing. **Yang Yu:** Data curation, Formal analysis, Investigation, Methodology, Writing – original draft. **Xingchi Zhou:** Data curation, Software, Writing – review & editing. **Wei Zhou:** Data curation, Formal analysis, Software, Writing – review & editing. **Qijun Pei:** Data curation, Formal analysis, Writing – review & editing. **Khai C. Tan:** Formal analysis, Writing – review & editing. **Anan Wu:** Data curation, Formal analysis, Software, Writing – review & editing. **Hui Wu:** Formal analysis, Software, Writing – review & editing. **Teng He:** Conceptualization, Funding acquisition, Project administration, Supervision, Validation, Writing – review & editing. **Ping Chen:** Conceptualization, Formal analysis, Funding acquisition, Methodology, Project administration, Supervision, Writing – review & editing.

Declaration of competing interest

The authors declare that they have no known competing financial interests or personal relationships that could have appeared to influence the work reported in this paper.

Acknowledgments

Appendix A. Supplementary material

Supplementary data to this article can be found online at https://doi.org/10.1016/j.jechem.2024.12.001.

References

[1] L. Schlapbach, A. Züttel, Nature 414 (2001) 353–358.
[2] D. Forberg, T. Schwob, M. Zaheer, M. Friedrich, N. Miyajima, R. Kempe, Nat. Commun. 7 (2016) 1–6.
[3] T. Autrey, P. Chen, J. Energy Chem. 77 (2023) 119–121.
[4] P. Preuster, C. Papp, P. Wasserscheid, Acc. Chem. Res. 50 (2017) 74–85.
[5] P.M. Modisha, C.N.M. Ouma, R. Garidzirai, P. Wasserscheid, Energy Fuel 33 (2019) 2778–2796.
[6] M.D. Allendorf, V. Stavila, J.L. Snider, M. Witman, M.E. Bowden, K. Brooks, B.L. Tran, T. Autrey, Nat. Chem. 14 (2022) 1214–1223.
[7] M. Navlani-García, K. Mori, Y. Kuwahara, H. Yamashita, NPG Asia Mater. 10 (2018) 277–292.
[8] Y. Liu, W. Zhang, X. Zhang, L. Yang, Z. Huang, F. Fang, W. Sun, M. Gao, H. Pan, Renew. Sustain. Energy Rev. 184 (2023) 113560.
[9] A. Schneemann, J.L. White, S. Kang, S. Jeong, L.F. Wan, E.S. Cho, T.W. Heo, D. Prendergast, J.J. Urban, B.C. Wood, M.D. Allendorf, V. Stavila, Chem. Rev. 118 (2018) 10775–10839.
[10] C. Lang, Y. Jia, X. Yao, Energy Storage Mater. 26 (2020) 290–312.
[11] T. He, H. Cao, P. Chen, Adv. Mater. 31 (2019) 1902757.
[12] M.J. Zhou, Y. Miao, Y. Gu, Y. Xie, Adv. Mater. 20 (2024) 202311355.
[13] T. He, Q. Pei, P. Chen, J. Energy Chem. 24 (2015) 587–594.
[14] G. P. Pez, A. R. Scott, A. C. Cooper, H.Cheng, F.C.Wilhelm, A. H. Abdourazak, US7351395B1.
[15] E. Clot, O. Eisenstein, R.H. Crabtree, Chem. Commun. 22 (2007) 2231–2233.
[16] Y. Yu, T. He, A. Wu, Q. Pei, A. Karkamkar, T. Autrey, P. Chen, Angew. Chemie - Int. Ed. 58 (2019) 3102–3107.
[17] K.C. Tan, Y. Yu, R. Chen, T. He, Z. Jing, Q. Pei, J. Wang, Y.S. Chua, A. Wu, W. Zhou, H. Wu, P. Chen, Energy Storage Mater. 26 (2020) 198–202.
[18] K.C. Tan, Z. Jing, Y. Yu, Y.S. Chua, Q. Pei, D. Zheng, X. Zhang, Z. Ge, F. Zhang, T. He, Int. J. Hydrogen Energy 46 (2021) 11051–11058.
[19] Z. Jing, Q. Yuan, Y. Yu, X. Kong, K.C. Tan, J. Wang, Q. Pei, X.-B. Wang, W. Zhou, H. Wu, A. Wu, T. He, P. Chen, ACS Mater. Lett. 3 (2021) 1417–1425.
[20] T. He, H. Cao, P. Chen, Accounts Mater. Res. 2 (2021) 726–738.
[21] Y. Cui, S. Kwok, A. Bucholtz, B. Davis, R.A. Whitney, P.G. Jessop, New J. Chem. 32 (2008) 1027–1037.
[22] J. Wu, I. Ying Zhang, X. Xu, ChemPhysChem 11 (2010) 2561–2567.
[23] C.R. Crecca, A.E. Roitberg, J. Phys. Chem. A. 110 (2006) 8188–8203.
[24] A.R. Kottaichamy, S. Begum, M.C. Devendrachari, Z.M. Bhat, R. Thimmappa, H. M. Nimbegondi Kotresh, C.P. Vinod, M.O. Thotiyl, Anal. Chem. 92 (2020) 4541–4547.
[25] S.J. Blanksby, G.B. Ellison, Acc. Chem. Res. 36 (2003) 255–263.
[26] R.G. Parr, Z. Zhou, Acc. Chem. Res. 26 (1993) 256–258.
[27] M.Kunert, E.Dinjus, M.Nauck, J.Sieler CCDC 107631: Experimental Crystal Structure Determination, 1998, DOI: 10.5517/cc3lzzm.
[28] F. Glorius, N. Spielkamp, S. Holle, R. Goddard, C.W. Lehmann, Angew. Chem. Int. Ed. 43 (2004) 2850–2852.
[29] L. Hegedűs, K. Szőke-Molnár, I.E. Sajó, D.F. Srankó, Z. Schay, Catal. Lett. 148 (2018) 1939–1950.